

# The hunt for the Kármán “constant” revisited

Peter A. Monkewitz<sup>1</sup>† and Hassan M. Nagib<sup>2</sup>

<sup>1</sup>École Polytechnique Fédérale de Lausanne (EPFL), CH-1015, Lausanne, Switzerland

<sup>2</sup>Illinois Institute of Technology, Chicago, IL 60616, USA

(Received xx; revised xx; accepted xx)

The logarithmic law of the wall, joining the inner, near-wall mean velocity profile (abbreviated MVP) in wall-bounded turbulent flows to the outer region, has been a permanent fixture of turbulence research for over hundred years, but there is still no general agreement on the value of the pre-factor, the inverse of the Kármán “constant”  $\kappa$ , or on its universality. The choice diagnostic tool to locate logarithmic parts of the MVP is to look for regions where the indicator function  $\Xi$  (equal to the wall-normal coordinate  $y^+$  times the mean velocity derivative  $dU^+/dy^+$ ) is constant. In pressure driven flows however, such as channel and pipe flow,  $\Xi$  is significantly affected by a term proportional to the wall-normal coordinate, of order  $\mathcal{O}(\text{Re}_\tau^{-1})$  in the inner expansion, but moving up across the overlap to the leading  $\mathcal{O}(1)$  in the outer expansion. Here we show, that due to this linear overlap term,  $\text{Re}_\tau$ ’s of the order of  $10^6$  and beyond are required to produce one decade of near constant  $\Xi$  in channels and pipes. The problem is resolved by considering the common part of the inner asymptotic expansion carried to  $\mathcal{O}(\text{Re}_\tau^{-1})$ , and the leading order of the outer expansion. This common part contains a *superposition* of log law and linear term  $L_0 y^+ \text{Re}_\tau^{-1}$ , and corresponds to the linear part of  $\Xi$ , which, in channel and pipe, is concealed up to  $y^+ \approx 500 - 1000$  by terms of the inner expansion. The approach provides a new and robust method to simultaneously determine  $\kappa$  and  $L_0$  in pressure driven flows at currently accessible  $\text{Re}_\tau$ ’s, and yields  $\kappa$ ’s which are consistent with the  $\kappa$ ’s deduced from the Reynolds number dependence of centerline velocities. A comparison with the zero-pressure-gradient turbulent boundary layer, henceforth abbreviated “ZPG TBL”, further clarifies the issues and improves our understanding.

## 1. Introduction

The logarithmic law for the mean velocity in wall-bounded turbulent flows goes back to the celebrated work of von Kármán (1934) and Millikan (1938). This log-law is firmly rooted in the framework of matched asymptotic expansions (abbreviated MAE, see e.g. Kevorkian & Cole 1981; Wilcox 1995), where it represents a key term of the overlap layer between the inner and outer mean velocity expansions,  $U_{\text{in}}^+(y^+)$  and  $U_{\text{out}}^+(Y)$ . In the present paper, only the simplest stream-wise homogeneous cases of plane channel and pipe flow will be considered and compared to the ZPG TBL.

In the following, the standard non-dimensionalization is adopted, with the “inner” or viscous length scale  $\hat{\ell} \equiv (\hat{\nu}/\hat{u}_\tau)$ , where  $\hat{u}_\tau \equiv (\hat{\tau}_w/\hat{\rho})^{1/2}$ ,  $\hat{\rho}$  and  $\hat{\nu}$  are the friction velocity, density and dynamic viscosity, respectively, with hats denoting dimensional quantities. The resulting non-dimensional inner and outer wall-normal coordinates are  $y^+ = \hat{y}/\hat{\ell}$  and  $Y = y^+/\text{Re}_\tau$ , respectively, with  $\text{Re}_\tau \equiv \hat{\mathcal{L}}/\hat{\ell}$  the friction Reynolds number and  $\hat{\mathcal{L}}$  the outer length scale such as channel half width, pipe radius or boundary layer thickness.

† Email address for correspondence: peter.monkewitz@epfl.ch

A key term in the MVP overlap is the logarithm  $\kappa^{-1} \ln y^+$ , with  $\kappa$  the Kármán “constant”, or rather parameter, as its flow dependence is confirmed by the present work. By definition, this logarithm is, within the overlap, common to both the leading order inner and outer expansions, where it takes the form  $\kappa^{-1} [\ln Y + \ln \text{Re}_\tau]$ . It follows that

(i)  $\kappa$  can be equally well determined from  $U^+(y^+)$  or  $U^+(Y)$  as shown in this paper, and is not as trivial as it sounds.

(ii) Furthermore, if the outer expansion is of the well accepted form  $\kappa^{-1} [\ln Y + \ln \text{Re}_\tau]$  plus an  $\mathcal{O}(1)$  function of  $Y$  (see e.g. Coles 1956), plus terms of order  $\mathcal{O}(\text{Re}_\tau^{-1})$  and higher, the leading order centerline velocity in channels and pipes *must* be  $\kappa^{-1} \ln \text{Re}_\tau$  plus a constant, as discussed for instance in Nagib *et al.* (2017). It is noted in passing, that for the asymptotic matching of inner and outer expansions, the term  $\kappa^{-1} \ln \text{Re}_\tau$  has to be treated as an  $\mathcal{O}(1)$  term, as shown by Crighton & Leppington (1973). This equality of overlap and centerline  $\kappa$  could only be relaxed, if the outer expansion contained an additional  $\mathcal{O}(1)$  term proportional to  $[\exp(-\gamma/Y) \ln \text{Re}_\tau]$ , which becomes transcendently small for  $Y \rightarrow 0$  or an analogous inner term  $\propto \exp(-\gamma y^+)$  (see e.g. Wilcox 1995, for a discussion of transcendently small terms). Lacking any evidence for such terms, the  $\kappa$ ’s extracted from overlap profiles and from the  $\text{Re}_\tau$  dependence of the centerline velocity *must be identical* !

The choice tool to locate logarithmic regions, especially in mean velocity profiles obtained by DNS, where the velocity derivative is readily available, has been the log-indicator function

$$\Xi \equiv y^+ \frac{dU^+}{dy^+} \equiv Y \frac{dU^+}{dY} \quad (1.1)$$

which is constant whenever  $U^+$  is a linear function of  $\ln y^+$ . It is noted, however, that an interval of constant  $\Xi$  is not automatically an inner-outer overlap, as there are additional requirements in MAE, the most important being that the center of the overlap has to scale on the intermediate variable  $(y^+ Y)^{1/2}$ , and its extent has to expand with  $\text{Re}_\tau$ .

Traditionally, the MVP overlap has been determined by locating a region of constant  $\Xi$ . In technical MAE terms, this amounts to consider the basic  $(1\mathcal{O}\text{inner}/1\mathcal{O}\text{outer})$  common part, also called overlap. Here and in the following, “ $(n\mathcal{O}\text{inner}/m\mathcal{O}\text{outer})$  overlap”, is a shorthand for an overlap constructed from an inner asymptotic expansion of  $n$ -th order and its outer counterpart of  $m$ -th order. Considering the  $(1\mathcal{O}\text{inner}/1\mathcal{O}\text{outer})$  MVP overlap is perfectly legitimate, since, in terms of the intermediate overlap variable  $\eta = y^+ \text{Re}_\tau^{-1/2} = Y \text{Re}_\tau^{+1/2}$ , the linear term  $L_0 y^+ / \text{Re}_\tau$  is of order  $\mathcal{O}(\text{Re}_\tau^{-1/2})$  relative to the  $\mathcal{O}(1)$  log law and does therefore not appear in the  $(1\mathcal{O}\text{inner}/1\mathcal{O}\text{outer})$  overlap. In practice, however, this approach is not very helpful in the presence of an additional linear overlap term, such as in channels and pipes. In order to determine  $\kappa$  with an error below 1% from a region of sufficiently constant  $\Xi$ , extending to, say,  $y^+ = 10^4$ , a very large Reynolds number of  $\text{Re}_\tau \geq (10^6 \kappa L_0)$  is required. Ignoring this limitation has been the main reason for the lack of agreement on  $\kappa$  values.

The difficulties with this traditional approach stem from additional terms in the overlap region, discussed early on by Yajnik (1970) and Afzal & Yajnik (1973), among others. Of particular relevance is the linear term  $L_0 y^+ / \text{Re}_\tau$  in the  $U^+$  profile of channels and pipes, which represents an  $\mathcal{O}(\text{Re}_\tau^{-1})$  correction of the *inner-scaled* indicator function  $\Xi(y^+)$ , as discussed for instance by Jiménez & Moser (2007), Lee & Moser (2015, sec. 3.1) and Luchini (2017), who has argued that the coefficient  $L_0$  of this linear term

$L_0 y^+ / \text{Re}_\tau$  is proportional to the pressure gradient (see appendix B for a critical review of his derivation).

The purpose of this paper is to clarify both the location, extent and the functional form of the inner-outer overlap in channels and pipes, and to propose a novel robust method to extract  $\kappa$  from MVPs in pressure driven flows. A comparison with the zero-pressure-gradient turbulent boundary layer further clarifies the issues. The paper will focus on the following points :

(i) The problem of the non-negligible linear term in the overlap of channels and pipes is resolved by moving to the  $(2\mathcal{O}_{\text{inner}}/1\mathcal{O}_{\text{outer}})$  overlap, which includes the linear term  $L_0 y^+ / \text{Re}_\tau \equiv L_0 Y$ , because it is present in *both* the limit  $y^+ \rightarrow \infty$  of the inner expansion carried to the second order  $\mathcal{O}(\text{Re}_\tau^{-1})$  and the limit  $Y \rightarrow 0$  of the leading order outer expansion. This  $(2\mathcal{O}_{\text{inner}}/1\mathcal{O}_{\text{outer}})$  overlap corresponds to the *linear part*  $[\kappa^{-1} + L_0 Y]$  of the outer-scaled indicator function  $\Xi(Y)$ , which, up to  $y^+ \approx 10^3$ , is “buried” under an inner-scaled “hump”, clearly visible in figure 2 for channel and figure 5 for pipe flow. This supports the conclusion of Monkewitz (2021) about the “late start” of the channel overlap. Beyond  $y^+ \approx 10^3$ , the overlap  $[\kappa^{-1} + L_0 Y]$  of  $\Xi$  becomes clearly visible in these figures and is seen to extend to  $Y \approx 0.4 - 0.5$ .

(ii) From the above outer-scaled form of the overlap it follows conclusively, that the “hump” of  $\Xi$  on top of the linear overlap, seen in all the channel and pipe profiles below a  $y^+$  of roughly  $10^3$ , belongs to the *inner* expansion. Consequently, the short horizontal or near-horizontal parts of  $\Xi$  within this “hump”, seen for instance in Lee & Moser (2015, fig. 3), as well as in figures 2 and 5 of the present paper, are not overlap log laws, but locally logarithmic regions of the inner expansion.

(iii) The above interpretation of  $\Xi$  is complicated by a surprisingly large variability between different channel DNS, and even more so between pipe DNS. This variability has different sources, such as domain size, computational scheme and grid spacing. In section 2, the particular effect of grid spacing in the outer flow region is highlighted for channel DNS. The analysis suggests that there is a critical grid spacing  $\Delta y^+$  of 3 to 4, which, when exceeded towards the centerline, leads to a decrease of the effective  $\text{Re}_\tau$  in the central region of the channel (see figure 3 and discussion related to it).

(iv) The clarification of the relation between the  $\kappa$  value derived from the dependence of centerline velocity on  $\ln \text{Re}_\tau$  and the various  $\kappa$  values reported in the literature based on a logarithmic part of the MVP.

In section 2, an improved outer fit of the mean velocity derivative in channels is developed from DNS, with additional details provided in appendix A. The resulting outer fit of the indicator function  $\Xi$  is compared to different channel DNS and the variability of the results is correlated with the different choices of computational grid spacing.

The superposition of log law and linear term in the overlap is supported by the experimental data of Zanoun *et al.* (2003) and Schultz & Flack (2013) obtained in channels of aspect ratio  $\approx 8$ . The simultaneous determination of the two overlap parameters  $\kappa$  and  $L_0$  is performed with a new robust method, presented in figure 4.

Section 3 then presents an analysis of three pipe flow DNS by El Khoury *et al.* (2013), Pirozzoli *et al.* (2021) and Yao *et al.* (2023), which show considerable differences of  $\Xi(Y)$ . On the other hand, the  $\Xi$  for the Superpipe data of Zagarola & Smits (1998), McKeon (2003) and Bailey *et al.* (2013) are found to be very consistent, and the new method for the determination of overlap parameters yields  $\kappa = 0.43$  and  $L_0 = 2.5$  for the linear term.

In the brief section 4, the findings for channel and pipe flow are contrasted with the

ZPG TBL. The experimental data from three independent sources reveal that the TBL indicator function also features a linear part with a significantly higher slope than in channels and pipes, with the crucial difference that this linear part *starts* only in the *outer region* at  $Y = 0.11$ , and therefore does *not* belong to the overlap.

The final section 5 summarizes the main results and closes with observations on the universality, or rather non-universality, of the so-called canonical turbulent flows: ZPG TBL, channel and pipe flow.

Two appendices complete the paper: Appendix A provides more details on the fit of the channel MVP, used in section 2. Appendix B discusses different approaches, including the one by Luchini (2017), for taking into account the effect of pressure gradient in MVP overlap profiles.

## 2. The outer expansion and the overlap of the indicator function in channels

To prepare for the analysis of the channel indicator function, the outer mean velocity fit of Monkewitz (2021, equ. 3.6) is improved and simplified, while maintaining its basic ingredients. The differences to Monkewitz (2021) are that the fitting is started with the mean velocity *derivative*, the  $\kappa$  is slightly modified to 0.417, and the  $\mathcal{O}(\text{Re}_\tau^{-1})$  contribution to  $dU^+/dY$  is simplified :

$$\frac{dU^+}{dY} \Big|_{\text{outer fit}} = \frac{1}{\kappa Y} + L_0 + \frac{1}{\text{Re}_\tau} L_1 - \left\{ \frac{1}{\kappa} + L_0 + \frac{1}{\text{Re}_\tau} L_1 \right\} \frac{dW}{dY} \quad (2.1)$$

with

$$\kappa = 0.417, L_0 = 1.15, L_1 = 380 \quad \text{and} \quad \frac{dW}{dY} = \frac{\ln \{\exp[11(Y-0.73)]+1\}}{\ln \{\exp[11(1-0.73)]+1\}} \quad (2.2)$$

More details on this fit are provided in appendix A.

Starting with the velocity derivative has the advantage that, for the correct  $\kappa$ , the term  $dU_{\text{DNS}}^+/dY - (\kappa Y)^{-1}$  becomes locally constant in the overlap region, irrespective of the value of  $L_0$  in equation (2.1). This is clearly seen in figure 1(a), where  $(dU_{\text{DNS}}^+/dY) - (\kappa Y)^{-1}$  is constant in the range  $0.2 \lesssim Y \lesssim 0.45$  for  $\kappa = 0.417$  and Reynolds numbers beyond around 2000.

The choice of  $\kappa = 0.417$  fits the profile of Lee & Moser (2015) for  $\text{Re}_\tau = 5186$ , considered among the most reliable, particularly well and is within the estimated range of uncertainty for the  $\kappa$ 's deduced from centerline velocities in Monkewitz (2017, fig. 8) and Monkewitz (2021, fig. 6). The only profile in figure 1, which is not well fitted by  $\kappa = 0.417$ , is the  $\text{Re}_\tau = 10049$  profile of Hoyas *et al.* (2022). Possible reasons for this discrepancy are discussed in relation to figure 3.

In a second step from parts (a) to (b) of figure 1, the constants in equation (2.1),  $[1.15 + 380 \text{Re}_\tau^{-1}]$ , are subtracted, showing that the  $\mathcal{O}(\text{Re}_\tau^{-1})$  correction consistently reduces the spread between profiles of different  $\text{Re}_\tau$ . In the last step from parts (b) to (c) of figure 1, the derivative  $[\kappa^{-1} + 1.15 + 380 \text{Re}_\tau^{-1}](dW/dY)$  of the wake profile is subtracted, demonstrating the quality of the outer fit (2.1, 2.2).

How much one can be led astray when deducing Kármán “constants” from an inappropriate region of the indicator function (1.1) is demonstrated with figure 2, which compares the outer fit of  $\Xi$ , obtained from equations (2.1, 2.2), to the  $\Xi_{\text{DNS}}$  of the six highest  $\text{Re}_\tau$  cases of figure 1.

As already stated in the introduction, the outer expansion of  $\Xi$  contains the complete ( $2\mathcal{O}_{\text{inner}}/1\mathcal{O}_{\text{outer}}$ ) overlap consisting of log law plus the linear term  $L_0 y^+/\text{Re}_\tau \equiv L_0 Y$ . Therefore, the deviations of  $\Xi_{\text{DNS}}$  from their outer fit necessarily belong to the inner expansion and not to the overlap. In particular, the short, near-horizontal portions of  $\Xi$

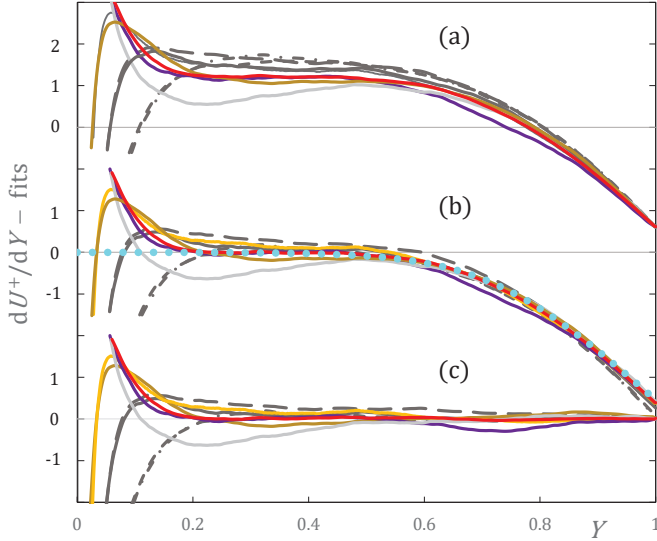


FIGURE 1. Successive approximations of mean velocity derivative  $dU_{\text{DNS}}^+ / dY$  for eight channel DNS:  $-\cdot-$  (grey),  $Re_\tau = 934$  (del Alamo *et al.* 2004);  $--$  (grey),  $Re_\tau = 1001$  (Lee & Moser 2015);  $-$  (grey),  $Re_\tau = 1995$  (Lee & Moser 2015);  $-$  (dark orange),  $Re_\tau = 3986$  (Yamamoto & Tsuji 2018);  $-$  (yellow),  $Re_\tau = 4079$  (Bernardini *et al.* 2014);  $-$  (red),  $Re_\tau = 5186$  (Lee & Moser 2015);  $-$  (violet),  $Re_\tau = 8000$  (Yamamoto & Tsuji 2018);  $-$  (light grey),  $Re_\tau = 10049$  (Hoyas *et al.* 2022). Panel (a):  $dU_{\text{DNS}}^+ / dY - (0.417 Y)^{-1}$ ; Panel (b): profiles in panel (a) minus constant  $(1.15 + 380 Re_\tau^{-1})$ ,  $\bullet\bullet\bullet$  (blue), wake fit  $[\kappa^{-1} + 1.15 + 380 Re_\tau^{-1}] (dW/dY)$  (equations 2.1, 2.2); Panel (c): profiles in panel (b) minus wake fit.

seen around  $y^+$  of 500 in figure 2, are not related to the overlap log law, but correspond to limited, approximately logarithmic *inner* regions (see also Monkewitz 2021, fig. 12).

The widespread association in the literature of these inner, nearly horizontal portions of  $\Xi$  with the inner-outer overlap has fueled years of controversy about the differences between  $\kappa$ 's determined from these features and from the  $Re_\tau$ -dependence of the centerline velocity. In addition it has led many authors to place the overlap layer in channels and pipes too close to the wall. To just cite a carefully documented example, Lee & Moser (2015, table 2 and fig. 3) estimated, for  $Re_\tau = 5186$ , a  $\kappa$  between 0.384 and 0.387 from the near-wall “hump” of  $\Xi$ , tantalizingly close to the well established  $\kappa$  of 0.384 for ZPG TBLs, reported by Monkewitz *et al.* (2007) and Nagib & Chauhan (2008), but significantly different from the centerline  $\kappa$ 's for the same data, shown in figure 8 of Monkewitz (2017), for instance.

Figure 2(a) also shows the boundaries of the  $(2\mathcal{O}_{\text{inner}}/1\mathcal{O}_{\text{outer}})$  overlap, defined as the locations, where the difference between  $\Xi_{\text{DNS}}$  and the linear overlap fit  $[\kappa^{-1} + (L_0 + L_1 Re_\tau^{-1}) Y]$  falls below a set value, taken here as 0.02. This choice results in an overlap starting at  $y^+ \approx 1200$  and ending at  $Y \approx 0.45$ , shown by green and red squares in figure 2. Note, that with the above criterion, the overlap for  $Re_\tau = 1995$  ends before it starts, which means that inner and outer expansions are not yet sufficiently separated to reveal the functional form of the overlap.

What is somewhat surprising in figure 2 are the rather large differences between the  $\Xi$ 's. The usual explanation is that, in terms of  $y^+$ ,  $\Xi$  is the product of a small and a large number. However, this is not so in terms of  $Y$ , which means that in current DNS practice, the outer part of the flow receives less, and possibly not enough attention compared to the near-wall part. Besides the size of the “computational box” and the

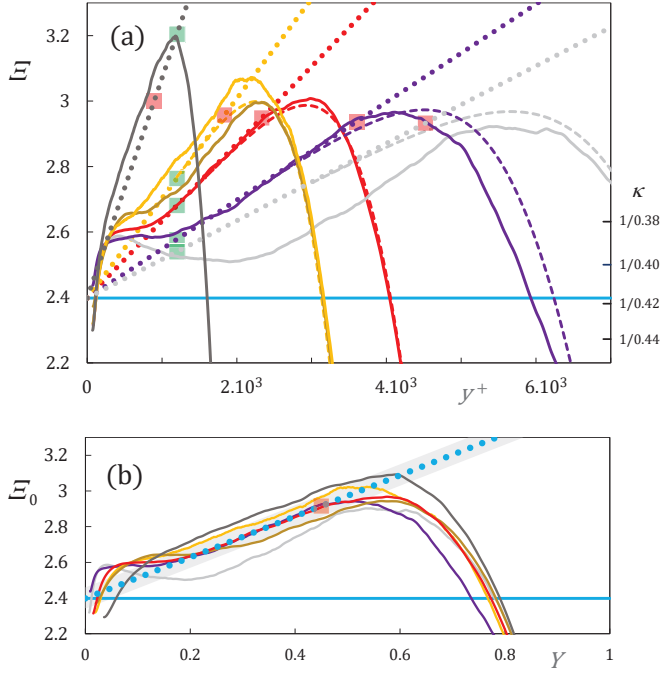


FIGURE 2. Channel indicator functions  $\Xi$  from DNS versus  $y^+$  and  $Y$ , for the six highest  $Re_\tau$  of figure 1 ( $Re_\tau = 1995$  and up). Same color scheme as in fig. 1. Panel (a): —,  $\Xi$  from DNS; ●●●, linear overlap fits  $[\kappa^{-1} + (L_0 + L_1 Re_\tau^{-1}) Y]$ ; - - -, complete outer fits of  $\Xi$  for  $Re_\tau = 4079$  and up (equations 2.1, 2.2). — (blue), (1/0.417). ■ (green),  $y^+ = 1200$  marking the approximate start of the overlap; ■ (red),  $Y = 0.45$  marking the approximate end of the overlap. Note that for the lowest  $Re_\tau = 1995$ , the overlap ends before it starts! Panel (b): DNS indicator functions minus higher order fits  $L_1 Y [1 - dW/dY]/Re_\tau$ ; ●●● (blue), leading order linear fit  $(1/0.417) + 1.15 Y$ ; grey band, variation of linear fit for  $\kappa = 0.417 \pm 0.01$

numerical scheme, the computational grid is a likely prominent culprit. This hypothesis is examined in figure 3, which shows the distribution of grid spacing  $\Delta y^+$  over the cross section for a number of channel flow DNS.

What is striking in this figure is the rapid increase of  $\Delta y^+$ , reaching 2 already at  $y^+ = 100$ , and reaching 10-15 on the centerline. The exceptions are the two DNS of Yamamoto & Tsuji (2018), where this increase is delayed to  $y^+ \approx 10^3$ . In the group of DNS without those of Yamamoto & Tsuji, the DNS of Lee & Moser (2015) for  $Re_\tau = 5186$  has the smallest  $\Delta y^+$ 's, while those of Hoyas *et al.* (2022) for  $Re_\tau = 10049$  are about twice as large, which has probably contributed to the “untypical”  $\Xi$  for this case in figure 2.

Unfortunately, the two DNS of Yamamoto & Tsuji (2018) have the largest  $\Delta y^+$ 's close to the wall and use a second order scheme, which leaves open questions. Nevertheless, the distribution of  $\Delta y^+$ 's may contribute to the explanation for the scatter in figure 2b. It is also evident in figure 3 that the  $\Xi$  of these two DNS change slope in the part that is linear in other DNS. The location of these slope changes, marked in the figure by large dots, correlates quite well with the location where the respective  $\Delta y^+$  reach a value of around 4.

As the slope of the linear part  $L_0 Y$  of  $\Xi$  is proportional to  $Re_\tau^{-1}$  in a graph of  $\Xi$  versus  $y^+$  (see equation 2.1), the steepening of the linear part of  $\Xi$  in figure 3 corresponds to a *decrease* of the effective Reynolds number. This phenomenon is well known from

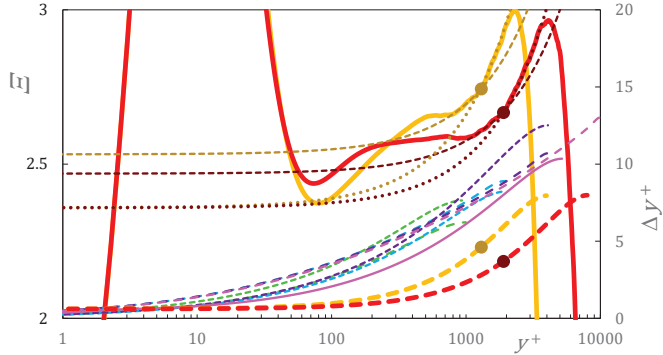


FIGURE 3. Grid spacing  $\Delta y^+$  of different channel DNS (right vertical axis) versus  $y^+$  compared to two indicator functions of Yamamoto & Tsuji (2018) (left axis).

*Left axis.* — (orange),  $\Xi(\text{Re}_\tau = 3986)$ ; ··· (light brown), linear fit  $(1/0.424) + 1.2 Y$ ; - - - (light brown), fit  $(1/0.395) + 0.65 Y$ ; • (light brown), switch between the two linear fits at  $y^+ \approx 1300$ . — (red),  $\Xi(\text{Re}_\tau = 8000)$ ; ··· (dark red), linear fit  $(1/0.424) + 1.3 Y$ ; - - - (dark red), fit  $(1/0.405) + 0.85 Y$ ; • (dark red), switch between the two linear fits at  $y^+ \approx 1900$ .

*Right axis.* Grid spacing for  $\text{Re}_\tau = 3986$  (thick orange dashes) and  $8000$  (thick red dashes) of Yamamoto & Tsuji (2018) with location of the change of linear slope of  $\Xi$  indicated by bullets. Comparison grid spacings shown for  $\text{Re}_\tau = 934$  (del Alamo *et al.* 2004, short green dashes),  $1001$  (Lee & Moser 2015, long green dashes),  $1995$  (Lee & Moser 2015, short blue dashes),  $2004$  (Hoyas & Jiménez 2006, long blue dashes),  $4079$  (Bernardini *et al.* 2014, long violet dashes),  $4179$  (Lozano-Durán & Jiménez 2014),  $5186$  (Lee & Moser 2015, pink solid line),  $10046$  (Hoyas *et al.* 2022, pink dashes).

the numerical integration of simpler equations, such as the diffusion equation, where an exaggerated rapid increase of the integration step results in a solution corresponding to a higher diffusivity. This suggests, that the grid spacing in the outer flow contributes significantly to the large differences of  $\Xi_0$  in figure 2b, and should probably be limited to  $\Delta y^+ \lesssim 3 - 4$ . However, the fidelity of a DNS to the true Navier-Stokes solution is also influenced by a number of other factors, such as statistical convergence (see for instance Vinuesa *et al.* 2016), the order of the numerical scheme, the computational box size, and the ratio of  $\Delta y$  to the Kolmogorov length, and further investigations are clearly called for.

Returning to the main subject of the paper, confirmation for the above analysis of the  $\Xi$  overlap in channel DNS is sought from experiment. Recognizing that experimental channels have a finite aspect ratio, one has to assume or hope that they provide MVPs that are reasonably close to DNS. Incidentally, channel DNS also use the approximation of span-wise periodicity for the infinite aspect ratio.

For comparison, the experimental data sets of Zanoun *et al.* (2003), using hotwires combined with the oil film technique to determine the wall skin friction, and Schultz & Flack (2013), using laser Doppler anemometry, obtained in channels of aspect ratio around 8 at  $\text{Re}_\tau$ 's in the same range as those of DNS in figure 2, have been analyzed and are shown in figure 4. The top two panels (a) and (b) of figure 4 show  $\Xi$  versus  $Y$  and an enlarged view of the wall region versus  $\log y^+$ . Panel (a) shows considerable scatter, due to the differentiation of experimental MVPs, but the linear range is rather clear between  $Y \approx 0.2$  and  $\approx 0.5$  with a slope of  $L_0 = 1.1$ , slightly less than the slope of 1.15, educed from channel DNS. Panel (b) shows the near-wall behavior of  $\Xi$  and clearly reveals a “hump” in the data of Zanoun *et al.* (2003) on top of  $1.1 Y$ , between  $y^+ \approx 100$  and close to  $10^3$ , similar to the “humps” in the DNS of figure 2. However, for unknown reasons, the data of Schultz & Flack (2013) lack such a “hump”.

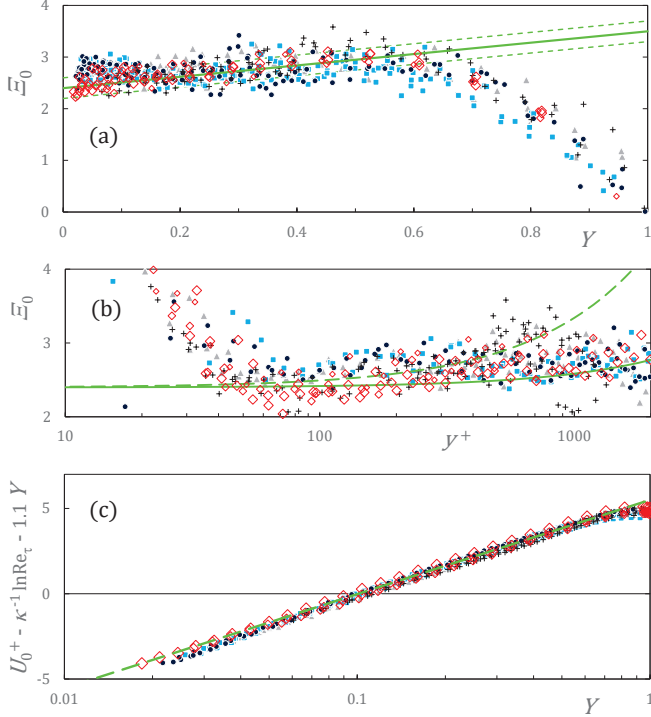


FIGURE 4. Indicator function  $\Xi(Y)$  and  $U_0^+(Y)$  minus linear part of overlap for two channel/duct experiments. The subscript “0” indicates that all data are corrected for finite Reynolds number effects with the  $\text{Re}_\tau^{-1}$  corrections in equations (2.1, 2.2, A 1, A 2). Hot wire data of Zanoun *et al.* (2003): + (black),  $\text{Re}_\tau = 1167, 1543, 1851$ ; ▲ (grey),  $\text{Re}_\tau = 2155, 2573, 2888$ ; ■ (blue),  $\text{Re}_\tau = 3046, 3386, 3698, 3903$ ; ● (dark blue),  $\text{Re}_\tau = 4040, 4605, 4783$ . LDA data of Schultz & Flack (2013): ◇ (red, increasing size),  $\text{Re}_\tau = 1010, 1956, 4048, 5895$ . (a)  $\Xi(Y)$ : — (green), linear fit  $(1/0.417) + 1.1 Y$  [note that the fitted  $L_0 = 1.1$  is slightly reduced relative to the best DNS fit in equation (2.2)]. - - - (green), linear laws with  $\kappa^{-1} = (1/0.417) \pm 0.2$ . (b) Blowup of  $\Xi$  versus  $y^+$ , with linear fits  $[(1/0.417) + 1.1 y^+/\text{Re}_\tau]$  for  $\text{Re}_\tau = 1167$  and 5895. (c) Corrected  $U_0^+(Y) - [(1/0.417) \ln \text{Re}_\tau + 1.1 Y]$ ; - - - (green), resulting log law  $(1/0.417) \ln Y + 5.5$ .

The third panel (c) of figure 4 is the “lynch pin” of the data analysis, demonstrating that, after removing the linear overlap term, a clear log law  $[(1/0.417) \ln \text{Re}_\tau + 5.5]$  emerges up to  $Y \approx 0.5$ . The “hump” below  $Y \approx 10^3 \text{Re}_\tau^{-1}$ , seen in figure 4b for the data of Zanoun *et al.* (2003), corresponds in figure 4c to the data which start to fall below the log law fit, i.e. onto a slope of higher  $\kappa^{-1}$ .

At first sight, one might think that figure 4c contains no new information, since  $\kappa$  is already used in the linear fit of  $\Xi_0$ . However, *only the slope* of  $\Xi_0$  is used and, when subtracting  $[\kappa^{-1} \ln \text{Re}_\tau]$  from  $U^+$ , a wrong  $\kappa$  only produces vertical  $\text{Re}_\tau$ -dependent shifts of the data sets, without affecting their logarithmic slope. Hence, this new method to determine the best fit  $\kappa$  in the presence of a linear overlap term is both robust and reliable. This assessment will be confirmed by the analogous analysis of the Superpipe data in the next section 3

### 3. The overlap of the indicator function in pipes

Starting again with DNS indicator functions for pipe flow, figure 5 has the same general shape as for the channel, with a clear linear region at higher  $\text{Re}_\tau$ , but a slope of about

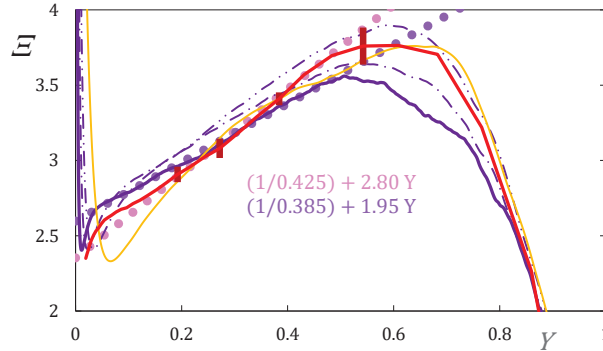


FIGURE 5. Indicator functions  $\Xi$  for selected pipe DNS: — (yellow),  $Re_\tau = 999$  of El Khoury *et al.* (2013); - - -, - - -, — (purple),  $Re_\tau = 1976, 3028$  and  $6019$  of Pirozzoli *et al.* (2021); — (red),  $Re_\tau = 5197$  of Yao *et al.* (2023), digitized from their figure 5(b), with selection of their uncertainty estimates. ● ● ● (purple), linear fit  $(1/0.40) + 2.2 Y$  of  $Re_\tau = 6019$  profile; ● ● ● (pink), linear fit  $(1/0.44) + 3.0 Y$  of  $Re_\tau = 5197$  profile.

twice the slope seen in figure 2 for the channel. In contrast to the channel, where the overlap of  $\Xi$  is quite well fitted by a unique leading order function  $(1/0.417) + 1.15 Y$  for of all but one DNS in figure 2, the  $\Xi$ 's for the pipe in figure 5 show more substantial differences between the DNS. One likely reason is the difference of computational schemes - finite differences for the profiles of Pirozzoli *et al.* (2021) and spectral elements for those of El Khoury *et al.* (2013) and Yao *et al.* (2023). In addition, the handling of the centerline grid singularity and the order of the numerical scheme may also have contributed to these differences.

As seen in figure 5, the linear portion of the data of Pirozzoli *et al.* (2021) for  $Re_\tau = 6019$  is quite well fitted by  $[(1/0.40) + 2.2 Y]$ , while the most recent data of Yao *et al.* (2023) are better fitted by  $[(1/0.44) + 3Y]$  in the range  $0.2 \leq Y \leq 0.5$ . These discrepancies between pipe DNS are clearly more serious than in channels and do not allow us to determine a pipe  $\kappa$  from the DNS results with any confidence. For this reason, one has to turn to experiments.

Specifically, we focus on the Superpipe data (Zagarola & Smits 1998; McKeon 2003; Bailey *et al.* 2013) that are probably the most scrutinized experimental data in turbulence history. Starting with the centerline, the Superpipe data are the only recent data set with a sufficient Reynolds number range to allow a fairly reliable estimate of  $\kappa$  from the  $Re_\tau$  dependence of centerline velocity. While the near-wall Pitot data have been the object of numerous challenges and corrections (see for instance Vinuesa & Nagib 2016), the centerline velocities have remained virtually unaffected and allows  $\kappa$  to be determined from  $U_{CL}^+(Re_\tau)$ . In Monkewitz (2017, fig. 4) the quality of the fit with the original  $\kappa = 0.436$  of Zagarola & Smits (1998) was found to be comparable to the one with  $\kappa = 0.42$ , deduced by McKeon (2003), but the comparative study of Nagib *et al.* (2017) suggests, that the pipe  $\kappa$  is closer to the original  $\kappa = 0.436$  of Zagarola & Smits (1998) than to 0.42.

Since pipe flow is pressure driven like channel flow, it is natural to use the methodology of section 2 to determine the pipe overlap parameters  $\kappa$  and  $L_0$ . The Superpipe data, corrected according to Bailey *et al.* (2013), are shown in figure 6 in the same format as the channel data in figure 4. The indicator function  $\Xi$ , shown in panel (a) of the figure, has a clear linear part, well fitted by  $[(1/0.44) + 2.5 Y]$ , which extends to  $Y \approx 0.45$ . The enlarged view of  $\Xi$  in panel (b) versus  $y^+$  shows again the “hump” of  $\Xi$  between  $y^+ \approx 10^2$

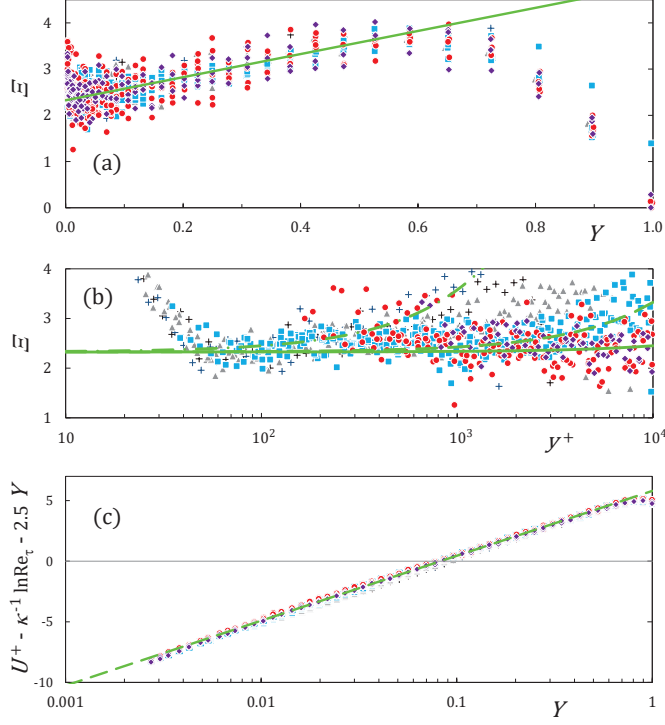


FIGURE 6. Indicator function  $\Xi(Y)$  and  $U^+(Y)$  minus linear part of overlap for the Superpipe data of McKeon (2003); Bailey *et al.* (2013). + (black),  $Re_\tau < 5.10^3$ ; ▲ (grey),  $5.10^3 < Re_\tau < 10^4$ ; ■ (blue),  $10^4 < Re_\tau < 5.10^4$ ; ● (red),  $5.10^4 < Re_\tau < 2.10^5$ ; ◆ (purple),  $2.10^5 < Re_\tau < 5.3 10^5$ .

(a)  $\Xi(Y)$ : — (green), linear fit  $(1/0.43) + 2.5 Y$ . (b) Blowup of  $\Xi$  versus  $y^+$ , with linear fits  $[(1/0.43) + 2.5 y^+ / Re_\tau]$  for  $Re_\tau = 2000, 25'000$  and  $250'000$ . (c)  $U^+(Y) - [(1/0.43) \ln Re_\tau + 2.5 Y]$ ; - - - (green), resulting log law  $(1/0.43) \ln Y + 5.8$ .

and about  $10^3$ , similar to the “hump” in one set of experimental channel profiles and in all channel and pipe  $\Xi$ ’s from DNS.

Due to the differentiation of experimental data, the scatter of  $\Xi$  is relatively large, and the uncertainty of the intercept is estimated at  $[0.44 \pm 0.03]^{-1}$ . However, as already made clear in section 2, only the slope  $L_0$  of  $\Xi$  is needed to determine  $\kappa$  from the logarithmic slope in figure 6c. This last figure shows a remarkable data collapse onto the log law  $[(1/0.43) \ln Y + 5.8]$  over about half the pipe radius, with an estimated uncertainty in  $\kappa$  of  $\pm 0.01$ . Furthermore, no Reynolds number trend of the linear slope  $L_0$  can be detected over the entire range of the Superpipe Reynolds numbers !

Significantly, the slope of the linear overlap term, obtained from the pipe profiles of this section, is roughly twice the slope in the channel overlap profile. This supports the basic finding of Luchini (2017), that, for sufficiently small pressure gradients,  $L_0$  is proportional to the pressure gradient parameter  $\beta \equiv -(\widehat{\mathcal{L}}/\widehat{\tau_w})(d\widehat{p}/d\widehat{x})$ , equal to 1 and 2 for channels and pipes, respectively. His dimensional analysis was however unnecessarily constrained, as discussed in appendix B.

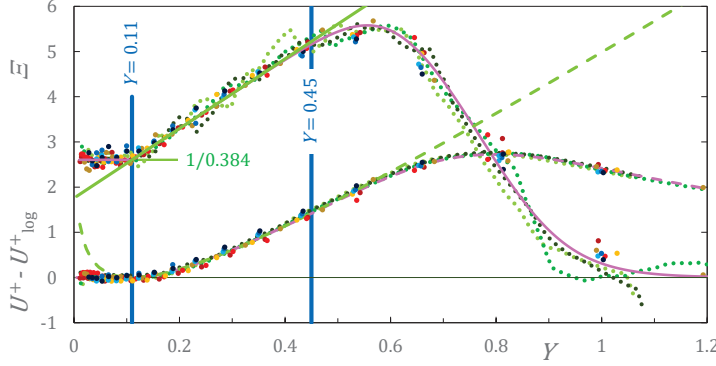


FIGURE 7. ZPG TBL Indicator function  $\Xi(Y)$  (top) and  $U^+(Y)$  minus log law  $[(1/0.384) \ln y^+ + 4.17]$  (bottom). • (yellow, dark yellow, red, dark red), data of Samie *et al.* (2018) for  $Re_\tau = 6, 10, 14.5 \& 20 \times 10^3$ . • (light blue, blue, dark blue), data of Österlund (1999) for  $Re_\tau = 5.5, 6.6 \& 7.9 \times 10^3$ . • • • (increasingly dark green), data of Nagib *et al.* (2007) for  $Re_\tau = 12.6, 16 \& 22.5 \times 10^3$  (for this last set, the log law constant has been increased from 4.17 to 4.32). Fits: — (light blue),  $\Xi = 1/0.384$ ; — (light green), linear part  $\Xi = (1/0.384) + 7.7(Y - 0.11)$  for  $0.11 \leq Y \lesssim 0.45$ ; — (lavender), full fit of  $\Xi$  (equations 4.1,4.2); - - - (light green), fit  $7.7[Y - 0.11 - 0.11 \ln(Y/0.11)]$  corresponding to the linear part of  $\Xi$ . - - - (lavender), full fit of  $U^+ - \log$  (num. integration of equations 4.1,4.2).

#### 4. Comparison to the outer MVP in the ZPG TBL

According to Luchini (2017), the ZPG TBL is the only one of the three “canonical” flows considered in the present paper, in which the overlap is a pure log law without a linear component. This is confirmed by the top part of figure 7, which shows  $\Xi$  obtained from the three experimental data sets of Samie *et al.* (2018), Österlund (1999) and Nagib *et al.* (2007) (note that for the latter two data sets, the  $Re_\tau$  values have been rescaled to match the definition of boundary layer thickness by Samie *et al.*).

The striking difference to figures 4a and 6a is the clean overlap log law, with the widely accepted best fit  $\kappa = 0.384$  of Monkewitz *et al.* (2007), which ends abruptly at the outer wall distance  $Y = 0.11$ .

The next part of  $\Xi(Y)$  in figure 7, between  $Y = 0.11$  and  $\approx 0.45$  is linear, with a large slope of 7.7. As this linear part starts only at a fixed outer location, it has nothing to do with the overlap and its physical origin is different. One likely candidate is the entrainment of free stream fluid into the boundary layer, as discussed by Chauhan *et al.* (2014a,b), for instance. The part of  $\Xi$  beyond  $Y \approx 0.45$  represents the transition to the free stream where  $\Xi = 0$ .

Both logarithmic overlap and linear part of  $\Xi$  are seen in the bottom part of figure 7 to provide, upon integration, an excellent outer fit of the MVP up to  $Y \approx 0.45$ . As the clear division of the outer  $\Xi$  into constant and linear parts appears more physical than the classical wake formulation of Coles (1956), the following full fit has been developed

$$\Xi(Y)|_{\text{outer fit}} = \left\{ \frac{1}{\kappa} + L(Y - Y_{\text{break}}) \mathcal{H}(Y - Y_{\text{break}}) \right\} \left\{ 1 - Y \frac{dW}{dY} \right\} \quad (4.1)$$

with  $\mathcal{H}$  the Heaviside function,  $\kappa = 0.384$ ,  $L = 7.7$ ,  $Y_{\text{break}} = 0.11$  and

$$Y \frac{dW}{dY} = \left\{ \frac{1}{19} \ln [1 + e^{19(Y-0.59)}] - \frac{1}{15} \ln [1 + 2e^{15(Y-0.92)}] \right\} \times \left\{ 0.92 - 0.59 - \frac{\ln 2}{15} \right\}^{-1} \quad (4.2)$$

which is easily integrated numerically to yield an excellent outer fit of the MVP in ZPG TBLs, as demonstrated by the dashed lavender curve in the lower part of figure 7.

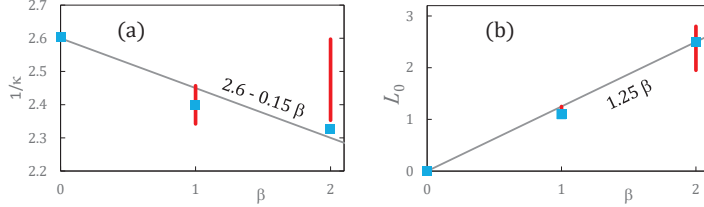


FIGURE 8. Dependence of the overlap parameters  $\kappa^{-1}$  and  $L_0$  (the slope of the linear term) on the pressure gradient parameter  $\beta \equiv -(\widehat{\mathcal{L}}/\widehat{\tau}_w)(d\widehat{p}/d\widehat{x})$ , equal to 1 and 2 for channel and pipe. Red  $\bullet$  and vertical ranges deduced from the DNS of figures 2 and 5; blue  $\blacksquare$ , best fits of the experimental data of figures 7, 4 and 6. — (grey), tentative linear fits.

## 5. Conclusions

The main conclusion of the present study is that the overlap of the MVP in channels, pipes and ZPG TBL's is not universal. This non-universality includes the overlap parameters, as well as the start or end locations. This non-universality should however not come as a surprise, as the MVP overlap provides the transition between the near-universal part of the profile in the inner, near-wall region and the geometry dependent outer part of the profile. How close to universal the inner parts of the MVP in ZPG TBLs, channels and pipes really are, still remains to be investigated more thoroughly. At any rate, they could only be strictly universal in the limit of  $Re_\tau \rightarrow \infty$ , since the Taylor expansion of  $U^+$  about the wall contains the higher order term  $\beta (2 Re_\tau)^{-1} (y^+)^2$  which depends on pressure gradient parameter  $\beta$  (see e.g. Monkewitz 2021, sec. 3.3).

### Specific results of the present analysis :

- (i) The overlap in channels and pipes does not start until  $y^+ = \mathcal{O}(10^3)$ , as already discussed by Monkewitz (2021). This follows from the *outer* expansion of the indicator function  $\Xi$  which must contain the overlap and, for small  $Y$ , is a simple linear function of  $Y$ .
- (ii) The (1*O*inner/1*O*outer) overlap of the MVP, i.e. the pure log law, is not useful in channel and pipe flow, since extreme Reynolds numbers are required to render it detectable over an extended wall distance.
- (iii) We have demonstrated, that, to remedy this problem, which is specific to channel and pipe flow, and more generally to flows with stream-wise pressure gradient, one has to resort to the (2*O*inner/1*O*outer) overlap, which contains, in addition to the log law, the linear term  $L_0(y^+/Re_\tau) \equiv L_0 Y$  (see also the discussion in section 1). This (2*O*inner/1*O*outer) overlap is clearly seen in channels and pipes for  $Re_\tau \gtrsim 5.10^3$  and extends from  $y^+ \approx 10^3$  to  $Y \approx 0.5$  with its center located at the intermediate variable  $(y^+Y)^{1/2} \approx 20 - 25$ . Based on these findings, a new method has been developed to extract both  $\kappa$  and  $L_0$  from MVPs. The present estimates for the dependence of these parameters on the pressure gradient parameter  $\beta \equiv -(\widehat{\mathcal{L}}/\widehat{\tau}_w)(d\widehat{p}/d\widehat{x})$ , equal to 1 and 2 for channel and pipe, are summarized in figure 8.
- (iv) As opposed to channel and pipe flows, the outer expansions of  $\Xi$  and  $U^+$  in the ZPG TBL feature a clear overlap log law with  $\kappa = 0.384$ , which ends at  $Y = 0.11$  (using the definition of Samie *et al.* (2018) for the boundary layer thickness). Beyond the overlap, a linear part of the outer  $\Xi$  has been identified in the interval  $Y \in [0.11, 0.45]$ , followed by the transition to the free stream. A new outer fit with these features has also been presented in section 4.
- (v) Regarding DNS, more higher quality channel and pipe DNS at  $Re_\tau$ 's around  $10^4$  with an increased attention to the accuracy of the outer flow are required to narrow down

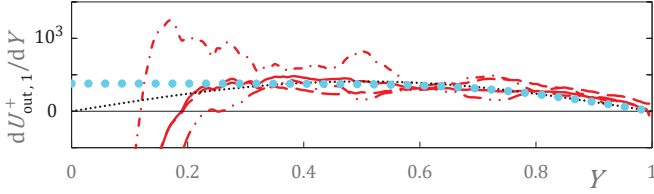


FIGURE 9. Contributions of order  $\mathcal{O}(\text{Re}_\tau^{-1})$  to the channel  $dU^+/dY$ , taken from figure 4b of Monkewitz (2021).  $\bullet\bullet\bullet$  (blue), new fit (2.1, 2.2);  $\cdots$  (black), previous fit in Monkewitz (2021).

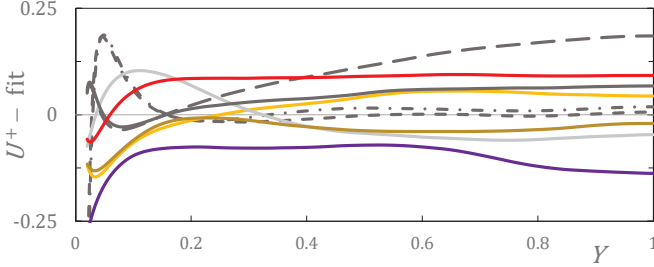


FIGURE 10. DNS mean velocity for the channel DNS of figure 1, minus the integral (A 1, A 2) of the outer fit (2.1, 2.2). Same color scheme as in figure 1.

the values of the overlap parameters in channel and pipe flows and to fully clarify their asymptotic structure. Increasing the accuracy of MVPs should have absolute priority over attempts to reach new record Reynolds numbers. It may also be interesting to perform DNS of high Reynolds number flows situated somewhere between channel and pipe flow, i.e. in rectangular or elliptic ducts of different aspect ratio, similar to the simulations of Vinuesa *et al.* (2018) at low  $\text{Re}_\tau$ 's.

We are grateful to Ricardo Vinuesa for sharing his expertise in DNS, which is reflected in the discussion around figure 3.

## Appendix A. Additional information on the outer expansion of the channel MVP in section 2

In section 2, the step from figure 1a to 1b involved the subtraction of contributions of  $\mathcal{O}(\text{Re}_\tau^{-1})$ . In Monkewitz (2021), this higher order correction for the velocity derivative was modelled by a  $\sin(\pi Y)$  function, reproduced here in figure 9. This fit has been simplified in equation (2.1). The simplified  $\mathcal{O}(\text{Re}_\tau^{-1})$  fit is seen in figure 9 to be equivalent to the previous one, except for  $Y \lesssim 0.2$  where it cannot be deduced from DNS at currently available  $\text{Re}_\tau$ 's.

To further validate the present outer expansion of the mean velocity derivative, the fit (2.1, 2.2) is integrated to

$$U_{\text{outer fit}}^+ = \frac{\ln Y}{\kappa} + \frac{\ln \text{Re}_\tau}{\kappa} + \left[ L_0 + \frac{L_1}{\text{Re}_\tau} \right] Y - \left[ \frac{1}{\kappa} + L_0 + \frac{L_1}{\text{Re}_\tau} \right] W + \left[ B_0 + \frac{B_1}{\text{Re}_\tau} \right] \quad (\text{A } 1)$$

$$\text{with } B_0 = 5.45, B_1 = -250 \quad (\text{A } 2)$$

The MVPs of the channel DNS used in figure 1 minus the outer fit (A 1, A 2) are shown in figure 10 to collapse rather well on the aggregate, although individual profiles could obviously be better fitted with slight adjustments of the parameters. For  $\text{Re}_\tau$ 's beyond  $10^3$ , the differences between DNS and the outer fit are below 0.5% of centerline velocities,

all the way to the inner boundary of the overlap. The latter can be estimated from figure 10 to be around  $y^+ \approx 1000$  ( $Y \approx 0.15$  for the Reynolds numbers in this figure), in accord with the conclusions of Monkewitz (2021). The outer limit of the overlap is seen in figure 1 to be at  $Y \approx 0.4 - 0.45$ , with the exact value depending on the maximum deviation allowed between overlap and full profile.

## Appendix B. The effect of pressure gradient on the overlap profile - Lucchini's analysis and beyond

The result of Luchini (2017), that, for sufficiently small pressure gradients, the coefficient  $L$  of the linear term in the MVP overlap is proportional to the pressure gradient parameter  $\beta \equiv -(\hat{\mathcal{L}}/\hat{\tau}_w)(d\hat{p}/d\hat{x})$ , which equals 1 and 2 for channels and pipes, respectively, can be justified in different ways.

One possibility is to use the stream-wise mean momentum equation (B 1)

$$\frac{d}{dy^+} \left[ \text{Re}_\tau \nu_T \frac{dU^+}{dy^+} \right] + \frac{\beta}{\text{Re}_\tau} = 0 \quad (\text{B } 1)$$

with a scaled eddy viscosity  $\text{Re}_\tau \nu_T$ . Integrating (B 1) once, and switching to the outer coordinate  $Y$  yields

$$\nu_T \frac{dU^+}{dY} = -\beta Y - K \quad (\text{B } 2)$$

Integrating equation (B 2) once more with the simple (negative) turbulent viscosity  $\nu_T = -\ell Y$  yields

$$U^+(Y) = \frac{\beta}{\ell} Y + \frac{K}{\ell} \ln Y + C \quad , \quad (\text{B } 3)$$

where  $\ell$ ,  $K$  and  $C$  may depend on  $\beta$  and are simply related to the overlap part of the mean velocity derivative in equations (2.1,2.2) and of the mean velocity in equation (A 1). In other words, (B 3) is perfectly suited to describe all “canonical” overlap profiles.

As seen below, it is more general than the overlap derived by Luchini (2017), who used dimensional analysis for the derivation of the  $\beta$ -dependence of the overlap profile. However, he excluded the channel half-width or pipe radius from the list of variables for the application of the Buckingham  $\Pi$  theorem, while implicitly keeping the hydraulic diameter, which is inversely proportional to the pressure gradient. This resulted in a universal  $\kappa$ , coveted by generations of fluid mechanicians, but not consistent with experimental evidence (see e.g. Nagib & Chauhan 2008; Monkewitz 2017, 2021).

Completing Lucchini's list of variables with the channel half-width or the pipe radius  $\hat{\mathcal{L}}$  to  $\{\hat{U}_y, \hat{y}, \hat{u}_\tau, \hat{p}_x, \hat{\mathcal{L}}, \hat{\rho}\}$ , one readily obtains the functional relation  $\Pi_1 = f(\Pi_2, \Pi_3)$  between the three non-dimensional  $\Pi$ 's

$$\Pi_1 = \frac{\hat{y} \hat{U}_y}{\hat{u}_\tau} \quad , \quad \Pi_2 = -\hat{\mathcal{L}} \frac{\hat{p}_x}{\hat{\tau}_w} \equiv \beta \quad , \quad \Pi_3 = \frac{\beta \hat{y}}{\hat{\mathcal{L}}} \quad . \quad (\text{B } 4)$$

Linearizing  $\Pi_1 = f(\Pi_2, \Pi_3)$  around  $\beta = 0$  yields  $\Pi_1 = \kappa^{-1} + B \Pi_2 + C \Pi_3 + \mathcal{O}(\beta^2)$ . With  $\hat{\mathcal{L}} \hat{u}_\tau \hat{\nu}^{-1} \equiv \text{Re}_\tau$ , this relation integrates to the non-dimensional overlap profile

$$U_{\text{overlap}}^+ = \frac{1}{\kappa_0 + \kappa_1 \beta} \ln(y^+) + [B_0 + B_1 \beta] + \frac{\beta}{\text{Re}_\tau} [C_0 y^+ + C_1] + \mathcal{O}(\beta^2) \quad (\text{B } 5)$$

One readily identifies  $\beta C_0$  in equation (B 5) with the coefficient  $L_0$  in equations (2.1) and (2.2). The same result (B 5) may also be obtained with the matching procedure of Millikan (1938).

Declaration of Interests: The authors report no conflict of interest.

## REFERENCES

AFZAL, NOOR & YAJNIK, KIRIT 1973 Analysis of turbulent pipe and channel flows at moderately large reynolds number. *Journal of Fluid Mechanics* **61** (1), 23–31.

DEL ALAMO, J. C., JIMENEZ, J., ZANDONADE, P. & MOSER, R. D. 2004 Scaling of the energy spectra of turbulent channels. *J. Fluid Mech.* **500**, 135–144.

BAILEY, S. C. C., HULTMARK, M., MONTY, J. P., ALFREDSSON, P. H., CHONG, M. S., DUNCAN, R. D., FRANSSON, J. H. M., HUTCHINS, N., MARUSIC, I., McKEON, B. J., NAGIB, H. M., ÖRLÜ, R., SEGALINI, A., SMITS, A. J. & VINUESA, R. 2013 Obtaining accurate mean velocity measurements in high Reynolds number turbulent boundary layers using Pitot tubes. *J. Fluid Mech.* **715**, 642–670.

BERNARDINI, MATTEO, PIROZZOLI, SERGIO & ORLANDI, PAOLO 2014 Velocity statistics in turbulent channel flow up to  $Re_\tau=4000$ . *Journal of Fluid Mechanics* **742**, 171–191.

CHAUHAN, K., PHILIP, J., DESILVA, CH. M., HUTCHINS, N. & MARUSIC, I. 2014a The turbulent/non-turbulent interface and entrainment in a boundary layer. *J. Fluid Mech.* **742**, 119–151.

CHAUHAN, K., PHILIP, J. & MARUSIC, I. 2014b Scaling of the turbulent/non-turbulent interface in boundary layers. *J. Fluid Mech.* **751**, 298–328.

COLES, D. E. 1956 The law of the wake in the turbulent boundary layer. *J. Fluid Mech.* **1**, 191–226.

CRIGHTON, D. G. & LEPPINGTON, F. G. 1973 Singular perturbation methods in acoustics – diffraction by a plate of finite thickness. *Phil. Trans. R. Soc. Lond. A* **335**, 313.

EL KHOURY, GEORGE K., SCHLATTER, PHILIPP, NOORANI, AZAD, FISCHER, PAUL F., BRETHOUWER, GEERT & JOHANSSON, ARNE V. 2013 Direct numerical simulation of turbulent pipe flow at moderately high reynolds numbers. *Flow, Turbulence and Combustion* **91** (3), 475–495.

HOYAS, S. & JIMÉNEZ, J. 2006 Scaling of the velocity fluctuations in turbulent channels up to  $Re_\tau = 2003$ . *Phys. Fluids* **18**, 011702.

HOYAS, SERGIO, OBERLACK, MARTIN, ALCÁNTARA-ÁVILA, FRANCISCO, KRAHEBERGER, STEFANIE V. & LAUX, JONATHAN 2022 Wall turbulence at high friction reynolds numbers. *Phys. Rev. Fluids* **7**, 014602.

JIMÉNEZ, JAVIER & MOSER, ROBERT D 2007 What are we learning from simulating wall turbulence? *Phil. Trans. R. Soc. A* **365** (1852), 715–732.

VON KÁRMÁN, TH. 1934 Turbulence and skin friction. *J. Aero. Sci.* **1**, 1–20.

KEVORKIAN, J. & COLE, J. D. 1981 *Perturbation methods in applied mathematics*. Springer.

LEE, M. & MOSER, R. D. 2015 Direct numerical simulation of turbulent channel flow up to  $Re_\tau = 5200$ . *J. Fluid Mech.* **774**, 395–415.

LOZANO-DURÁN, A. & JIMÉNEZ, J. 2014 Effect of the computational domain on direct numerical simulations of turbulent channels up to  $Re_\tau = 4200$ . *Phys. Fluids* **26**, 011702.

LUCHINI, PAOLO 2017 Universality of the turbulent velocity profile. *Phys. Rev. Lett.* **118**, 224501.

McKEON, BEVERLEY J. 2003 High Reynolds number turbulent pipe flow. PhD thesis, Princeton University.

MILLIKAN, C. M. 1938 A critical discussion of turbulent flows in channels and circular tubes. In *Proc. 5th Int. Congr. Appl. Mech.*.. Wiley, NY.

MONKEWITZ, PETER A. 2017 Revisiting the quest for a universal log-law and the role of pressure gradient in “canonical” wall-bounded turbulent flows. *Phys. Rev. Fluids* **2**, 094602.

MONKEWITZ, PETER A. 2021 The late start of the mean velocity overlap log law at  $y^+ = \mathcal{O}(10^3)$  – a generic feature of turbulent wall layers in ducts. *Journal of Fluid Mechanics* **910**, A45 1–28.

MONKEWITZ, P. A., CHAUHAN, K. A. & NAGIB, H. M. 2007 Self-consistent high-Reynolds-number asymptotics for zero-pressure-gradient turbulent boundary layers. *Phys. Fluids* **19**, 115101.

NAGIB, H. M. & CHAUHAN, K. A. 2008 Variations of von Kármán coefficient in canonical flows. *Phys. Fluids* **20**, 101518.

NAGIB, H. M., CHAUHAN, K. A. & MONKEWITZ, P. A. 2007 Approach to an asymptotic state for zero pressure gradient turbulent boundary layers. *Phil. Trans. R. Soc. Lond. A* **365**, 755–770.

NAGIB, H. M., MONKEWITZ, P. A., MOSCOTELLI, L., FIORINI, T., BELLANI, G., ZHENG, X. & TALAMELLI, A. 2017 Centerline Kármán 'constant' revisited and contrasted to log-layer Kármán constant at CICLoPE. In *Proc. TSFP10, Chicago, USA* (ed. H. M. Nagib & A. J. Smits).

ÖSTERLUND, JENS M. 1999 Experimental studies of zero pressure-gradient turbulent boundary layer flow. PhD thesis, Kungl Tekniska Högskolan (Royal Institute of Technology), Sweden.

PIROZZOLI, SERGIO, ROMERO, JOSHUA, FATICA, MASSIMILIANO, VERZICCO, ROBERTO & ORLANDI, PAOLO 2021 One-point statistics for turbulent pipe flow up to  $re_\tau \approx 6000$ . *Journal of Fluid Mechanics* **926**, A28.

SAMIE, M., MARUSIC, I., HUTCHINS, N., FU, M. K., FAN, Y., HULTMARK, M. & SMITS, A. J. 2018 Fully resolved measurements of turbulent boundary layer flows up to  $Re_\tau = 20000$ . *Journal of Fluid Mechanics* **851**, 391–415.

SCHULTZ, M. P. & FLACK, K. A. 2013 Reynolds number scaling of turbulent channel flow. *Phys. Fluids* **25**, 025104–1–13.

VINUESA, RICARDO & NAGIB, HASSAN M. 2016 Enhancing the accuracy of measurement techniques in high reynolds number turbulent boundary layers for more representative comparison to their canonical representations. *European Journal of Mechanics - B/Fluids* **55**, 300–312, vortical Structures and Wall Turbulence.

VINUESA, RICARDO, PRUS, CEZARY, SCHLATTER, PHILIPP & NAGIB, HASSAN M. 2016 Convergence of numerical simulations of turbulent wall-bounded flows and mean cross-flow structure of rectangular ducts. *Meccanica* **51**, 3025–3042.

VINUESA, R., SCHLATTER, P. & NAGIB, H. M. 2018 Secondary flow in turbulent ducts with increasing aspect ratio. *Phys. Rev. Fluids* **3**, 054606.

WILCOX, D. C. 1995 *Perturbation Methods in the Computer Age*. DCW Industries, Inc.

YAJNIK, KIRIT S. 1970 Asymptotic theory of turbulent shear flows. *Journal of Fluid Mechanics* **42** (2), 411–427.

YAMAMOTO, YOSHINOBU & TSUJI, YOSHIOUKI 2018 Numerical evidence of logarithmic regions in channel flow at  $Re_\tau = 8000$ . *Phys. Rev. Fluids* **3**, 012602.

YAO, JIE, REZAEIRAVESH, SALEH, SCHLATTER, PHILIPP & HUSSAIN, FAZLE 2023 Direct numerical simulations of turbulent pipe flow up to  $Re_\tau \approx 5200$ . *Journal of Fluid Mechanics* **956**, A18.

ZAGAROLA, M. V. & SMITS, A. J. 1998 Mean-flow scaling of turbulent pipe flow. *J. Fluid Mech.* **373**, 33–79.

ZANOUN, E. S., DURST, F. & NAGIB, H. M. 2003 Evaluating the law of the wall in two-dimensional fully developed turbulent channel flows. *Phys. Fluids* **15**, 3079–3089.